Nuclear Instruments and Methods in Physics Research A 385 (1997) 385–390

NUCLEAR INSTRUMENTS & METHODS IN PHYSICS RESEARCH Section A

# Development, operation and analysis of bialkali antimonide photocathodes for high-brightness photo-injectors

A. di Bona[a,*], F. Sabary[a], S. Joly[a], P. Michelato[b], D. Sertore[b], C. Pagani[b], S. Valeri[c]

[a]*Commissariat à l'Energie Atomique, Centre de Bruyères-le-Châtel, B.P. 12, 91680 Bruyères-le-Châtel, France*
[b]*Istituto Nazionale di Fisica Nucleare, Laboratorio LASA, Via fratelli Cervi 201, 20090 Segrate (MI), Italy*
[c]*Istituto Nazionae di Fisica della Materia and Università di Modena, Via G. Campi 213/a, 41100 Modena, Italy*

Received 17 June 1996

**Abstract**

Different methods for the preparation of K–Cs–Sb photocathodes, suitable for electron sources in RF guns, are described in detail. The resulting material has been characterized by Auger depth profiling technique, and by its spectral response in the 250–600 nm range, as well. The results of lifetime experiments under operational and "laboratory" conditions are presented. The role of $CO_2$ in reducing the operational lifetime of the photocathodes and that of $O_2$ in improving the long-wavelength response are investigated.

## 1. Introduction

Since their discovery in the middle of the fifties, bialkali antimonides have been widely utilized as sensitive materials in radiation detectors and camera tubes technology. Several reviews on this topic are available in the literature [1,2]. New attention has been recently brought to these materials due to the application they could have as high-brightness, pulsed electron sources for radio-frequency (RF) electron guns [3–8]. Their high quantum efficiency (QE) at visible wavelengths, allows the extraction of high-charge electron bunches as the photocathode is illuminated by an intense and pulsed light beam, e.g. a doubled-frequency, mode-locked, Nd:YAG laser. The main drawback to the utilization of bialkali antimonides in laser driven RF guns is represented by the fast degradation of their photoemissive characteristics, due to the critical environmental conditions they are exposed in the accelerating RF cavities. More resistant photocathode materials have been developed [1,8–11], but they require ultraviolet laser drives, which in turn introduce a number of new problems concerning the stability of the quadrupled-frequency lasers.

The development and the optimization of a photo-injector necessitate expertise which spans over a wide field of interests (accelerator and laser technologies, materials science, surface analysis) which can hardly be found in a single laboratory. Therefore, we coordinated the specific competencies of our laboratories in order to face the complexity of the problem from a general point of view.

Since 1992, the ELSA high-power free-electron laser is operated in Bruyères-le-Châtel [12], which utilizes as electron source a bialkali antimonide photocathode. In this laboratory, several photocathode preparation procedures have been tested and developed. Here, we had the possibility of operating the photocathodes in the accelerator installation, giving us information about their lifetime under "real" working conditions. These conditions have been simulated at INFN-LASA in Milano, where research and development activities are going on in the context of the Tesla Test Facility (TTF) program, in particular on the photo-injector for the collider [13]. At INFM in Modena, a photocathode fabrication system is connected by a ultra-high vacuum (UHV) transfer device to a multitechnique surface analysis system [14,15].

Bialkali antimonides are very sensitive to residual gas pollution, thus we (temporarily) abandoned the idea of transfering the photocathodes between the different laboratories. On the other hand, we dedicated some work in standardizing the fabrication procedures in order to "virtually" transport the photocathodes under the form of a sequence of operations that should be exactly reproduced in the specific laboratory.

## 2. Fabrication and analysis techniques

### 2.1. Experimental procedure

Due to the large number of experimental parameters

* Corresponding author. Tel. +33 1 69265344, fax +33 1 69267024, e-mail alessandro.dibona@unimo.it.


*PII* S0168-9002(96)00809-1

involved in the formation of a ternary compound, a lot of work has been devoted in the determination of the most significant ones. Then, we looked for a procedure which, while keeping under control the minimal set of significative parameters, ensures a good compromise between reproducibility, endurance and quantum efficiency. The three recipes described in the following are the result of such a methodology. They have been tested in different laboratories, under slightly different experimental conditions, and they unfailingly produce a high quantum efficiency photocathode.

Due to the high sensitivity of these materials to any form of pollution, all the procedures concerning the photocathode fabrication, operation or analysis must be performed under ultra-high vacuum conditions (UHV). We fabricated bialkali photocathodes into purposely designed vacuum equipments, whose base pressure are in the low $10^{-11}$ mbar range.

Antimony has been sublimated from 99.9999% pure antimony powder. Alkali metal vapor has been produced by the high-temperature decomposition of alkali chromates ($K_2CrO_4$ and $Cs_2CrO_4$) in the presence of a reducent compound (ST101 by Saes Getters). Two kinds of thermal evaporators have been used, namely boron nitride (BN) crucibles, tested at Bruyères-le-Châtel and the Saes Getters dispensers, tested in the Milano and Modena Laboratories. The BN crucibles are indirectly heated by a Ta filament, and their temperatures are measured by thermocouples. The Saes Getters dispensers are Ni pipes having a trapezoidal cross section, which contain the evaporation material. The material exits through a slit which is made along the pipe and it is directly heated by a current flow of several amperes produced in the pipe itself. No differences due to the different evaporation sources have been observed neither during the photocathode formation, nor during its operation. The main difference between these two kind of sources consists in the amount of material we can charge in them (approximately 1 $cm^3$ in the crucibles, 0.1 $cm^3$ in the dispensers), and in their thermal time constant (30 min for the crucibles, 2 min for the dispensers).

The rate of evaporation was monitored just before each deposition by a quartz microbalance. No attempt has been made to correct the quartz readings for the different temperatures of the substrate and the quartz itself. This possibly results in large deviations between the quartz indication and the effective deposited material thickness. Even if the actual value of the evaporation rate remains undetermined, the quartz microbalance is useful for the long term calibration of the sources.

The Auger depth profiles were performed in the Modena Laboratory, where a UHV analysis chamber, equipped with standard surface science facilities (scanning Auger, $Ar^+$ depth-profiling, X-ray photoelectron spectroscopy), is connected by a UHV transfer device to a fabrication chamber. In this chamber, we have reproduced the various fabrication recipes onto suitable sample-holders made of the same material as the RF plugs, namely Mo (used in the ELSA experiment) and AISI 316LN stainless steel (proposed for the TTF experiment). The transfer operation between the fabrication and the analysis system takes only 2 or 3 min during which the total pressure does not exceed $3 \times 10^{-10}$ mbar. Auger spectra were collected by a single pass cylindrical mirror analyzer which operates in the first derivative mode. The modulation voltage was 6 V peak-to-peak. The exciting electron beam was coaxial to the analyzer's cylinders, operating at 3 keV, 600 nA over a 100 μm × 100 μm area. We considered the following Auger transitions: Mo MNN (186 eV), K LMM (252 eV), Sb MNN (454 eV), Cs MNN (563 eV) and Fe LMM (703 eV).

Depth profiling was achieved by an $Ar^+$ gun operating at 0.8 keV, 40 $\mu A/cm^2$. From the sputtering yields of the pure elements, we can estimate an erosion rate of $0.2 \pm 0.1$ nm/s.

### 2.2. Fabrication recipes

*Recipe 1 (R1)*: This recipe is currently used for the production of the photocathodes in the ELSA system at Bruyères-le-Châtel. Due to its high level of reproducibility, an automatic fabrication process has been developed. This permits the production of two photocathodes per day, limited by the high thermal inertia of the massive Mo RF-plug onto which the photoemissive material is deposited. The Mo substrate is baked at 450°C for several hours. Then, the substrate temperature is lowered to 110°C and 5 nm of Sb are evaporated at 0.1 nm/s deposition rate. Potassium is deposited at the same rate, and the photocurrent produced by a green He–Ne laser ($\lambda = 546$ nm) or a filtered Hg lamp ($\lambda = 532$ nm) is monitored. The evaporation is stopped when a maximum in the photocurrent is reached, typically after 20 nm of K evaporation. The same procedure is then applied for the Cs evaporation. The typical QE at 532 nm is 2.5%.

*Recipe 2 (R2)*. The following two recipes has been developed and tested in the laboratory of Milano. A stainless steel (AISI 316 LN) substrate is baked to 450°C for several hours and bombarded, after cooling at room temperature, with $Ar^+$ ions (3 keV, 2 A s/$cm^2$). While keeping the substrate temperature at 120°C, we deposited, successively, 5 nm of Sb at 0.5 nm/min and 3 nm of K at 1 nm/min. Then, Cs is deposited at 2 nm/min until the maximum in the photocurrent is reached. With this recipe, the maximum QE at 532 nm is lower than 2%.

*Recipe 3 (R3)*: A photocathode fabricated following the recipe 2 is heated to 230°C for 1 h. The temperature is then lowered to 120°C and K is evaporated at 1 nm/min until a maximum in the photocurrent is reached. The QE of the photocathode is around 5% at 532 nm.

### 2.3. Characterization of the photocathodes

Fig. 1 shows the Auger depth profiles of the three kinds of photocathodes. The film thickness is between 10 nm

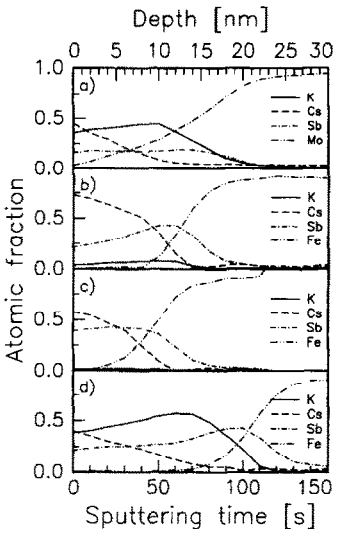


Fig. 1. Auger depth profiles of different photocathodes: (a) photocathode produced following R1; (b) photocathode produced following R2; (c) as (b), after 1 h at 230°C; (d) photocathode produced following R3.

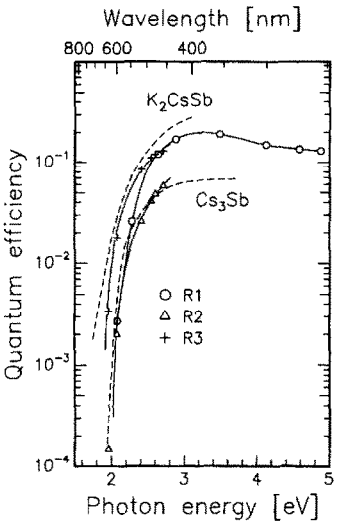


Fig. 2. Spectral responses of the photocathodes R1, R2 and R3. The spectral response of $Cs_3Sb$ and $K_2CsSb$ [1] is also reported for comparison.

(Figs. 1b and 1c) and 20 nm (Figs. 1a and 1d), remarkably less than the one we could calculate from the thickness of the deposited materials and the density of $K_2CsSb$. This is not surprising, since the sticking coefficient of the alkali atoms on the hot substrate is less than one and is different from that of the quartz, however.

Fig. 1a refers to a photocathode fabricated following the prescriptions of R1. The stoichiometric ratio between K and Sb is close to the expected value 2, over a region which extends as far as 12 nm below the surface. On the contrary, the Cs content decreases roughly linearly from about 0.5 at the surface to zero at 12 nm inside the film, indicating that the photoemissive material is not homogeneous in depth. The signal from the Mo substrate is detectable since the early stage of the erosion process, i.e. well before a film thickness corresponding to the escape depth of the Mo Auger electrons (~1 nm) is removed. This possibly indicates the presence of islands of photoemissive material which partially cover the substrate.

The depth profile of the photocathodes produced with the R2 procedure is shown in Fig. 1b. Potassium is diffused throughout the whole film, but its concentration level is well below the stoichiometric value of 50%. The film composition roughly changes from $Cs_3Sb$ at the surface, to CsSb at the substrate interface, being the presence of K to be considered as traces. In spite of the previous case, the substrate is completely covered by a photoemissive layer whose thickness is 10–15 nm.

The effects of the heat treatment at 230° are shown in Fig. 1c. We observe a depletion of the alkali metal components and an improvement in the film uniformity.

Recipe R3 gives rise to a photocathode whose depth profile is shown in Fig. 1d. If we compare it to that of Fig. 1a, we observe that they are very similar. The main difference consists in the behaviour of the substrate signal, which in this case shows a sharp transition at 20 nm from the surface. This indicates that the photoemissive film completely covers the substrate.

The spectral responses of the three photocathodes are shown in Fig. 2; for comparison, the curves relative to $Cs_3Sb$ and $K_2CsSb$ taken from the literature are indicated too.

The spectral response of the photocathode obtained from R1 is intermediate between that of $K_2CsSb$ and $Cs_3Sb$.

Recipe R2 gives essentially a $Cs_3Sb$ photocathode. On the other hand, the little amount of K evaporated (3 nm for R2 vs. 20–30 nm for R1 and R3) may be inadequate to form stoichiometric $K_2CsSb$, as the Auger depth profile of Fig. 1b points out. The spectral response of $K_2CsSb$ is quite exactly recovered by the subsequent K evaporation established by R3. The threshold energy varies from 2.0 to 1.9 eV, the latter is related to the stoichiometric $K_2CsSb$ compound.

## 3. Operation of the $K_2CsSb$ photocathodes

$K_2CsSb$ photocathodes have been used as electron sources in the RF gun of the ELSA free-electron laser at Bruyères-le-Châtel. A detailed description of the experiment can be found elsewhere [12], thus only a brief outline will be given here.

The electron beam in the ELSA accelerator is produced by illuminating the photocathode with a doubled-frequency Nd:YAG laser ($\lambda = 532$ nm). Experiments were performed with a typical macropulse length of 50 $\mu$s at a repetition rate of 1 Hz with 1 MW injected in the 144 MHz RF

cavity. During each macropulse, the laser drive delivers picosecond micropulses (whose duration may be chosen in the 20–60 ps range) on the photocathode surface at a repetition rate of 14.4 MHz. The maximum micropulse energy is about 5 $\mu$J.

The photocathodes are fabricated in a dedicated UHV chamber as prescribed by R1, and then transferred to the RF gun by means of a UHV actuator directly coupled to it. As mentioned before, the quantum efficiency at the end of the fabrication is typically 2.5%. The photocathodes can be stored in the fabrication chamber (base pressure in the low $10^{-10}$ mbar range) for several days without any drop in QE.

On the contrary, as the photocathode is working in the RF cavity, we observed a fast decay in QE, which effectively reduces the operational lifetime of the accelerator. The actual decay rate depends on several parameters, primarily on the amount of the injected RF power which in turn is responsible of the strong outgassing from the cavity walls. To get an idea about the operational conditions, the base pressure in the cavity was about $2 \times 10^{-9}$ mbar, which increases up to $8 \times 10^{-9}$ mbar when approximately 1 MW of RF power is injected. Under these conditions the lifetime (defined here as the time required to reduce the QE by a factor $e$) of the photocathode is approximately 1 h. To keep constant the amount of charge per electron bunch, the laser pulse energy is progressively increased as the QE of the photocathode decreases, until the maximum laser energy is reached, i.e. 5 $\mu$J per micropulse. For a bunch charge value of 1 nC, the operational time of the photocathode, i.e. the time during which we can extract the nominal charge, is approximately 4 or 5 h. If necessary, two photocathodes could be fabricated per day.

We performed few experiments to investigate the cause of the photocathode poisoning. To check the effects of the laser lightning alone, we brought the laser beam and the photocathode into the fabrication chamber, where the pressure is in the low $10^{-10}$ mbar range. The lifetime in these conditions was higher than 10 h, pointing out that the laser lighting has little or no influence on the photocathode operating life.

We have measured lifetimes of approximately 2 or 3 h when the photocathode is placed in the cavity without RF power and without laser illumination. Under these conditions, the base total pressure in the cavity was about $2 \times 10^{-9}$ mbar and the lifetime is ruled by the contamination of the surface by the residual gases.

Fig. 3 shows a mass spectrum of the residual gases in the cavity with and without RF power, between 10 and 50 mass units. RF power induces desorption of carbon monoxide, carbon dioxide and hydrocarbons. The partial pressure of water does not increase too much as the RF power is applied. One or several of these gases must be the cause of the very short photocathode lifetime during the photo-injector operation.

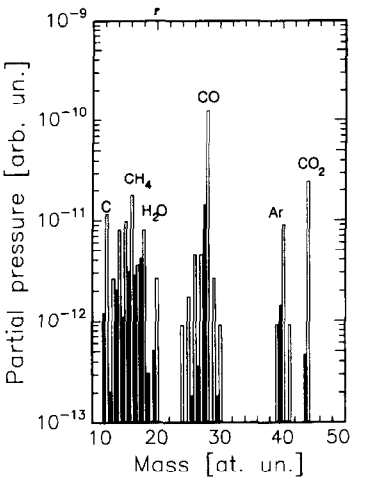


Fig. 3. Mass spectrum of the residual gas in the accelerating cavity without (solid) and with (outlined) 1 MW RF power. The spectrum is not corrected for the sensitivity factors of the different gases.

## 4. Exposition to different gases

We did lifetime experiments by exposing the photocathode to controlled quantities of pure gases for determining which of them are responsible for the short operational lifetime.

We measured the QE of the photocathodes prepared following R1 and R3, during the exposition to several pure gases, namely $CH_4$, $N_2$, CO, $O_2$ and $CO_2$. These experiments have been performed in the fabrication chamber, where no effects due to the residual gas contamination have been observed. The photocathodes have been exposed to the gases, one at a time, whose partial pressure was kept constant in the low $10^{-9}$ mbar range, i.e., a few Langmuirs [L] per hour (1 L corresponds to an exposition during 1 s at $1.31 \times 10^{-6}$ mbar). The gas purity has been checked by a quadrupole residual gas analyzer. For these experiments, we always used freshly prepared photocathodes, to avoid possible "historical" effects.

$CH_4$, $N_2$ and CO have no consequences on QE in the exposition range we explored, ie. $\approx 10^3$ L. At exposition values above this level, the contamination from the residual atmosphere cannot be excluded.

In Fig. 4 are shown the QE drops at 532 nm as a function of the exposition to $CO_2$ of the R1 and R3 photocathodes. The exposition levels which reduce to 1/e the QE are 2 L and 6 L for R1 and R3, respectively. During the photocathode operation, the total pressure is $8 \times 10^{-9}$ mbar, whose approximately 90% are CO, $CH_4$, hydrocarbons and Ar, the remaining 10% is $CO_2$, as Fig. 3 points out. The former have no effect on the photocathode lifetime. Thus, the sole active gas the photocathode is exposed during the operation is $CO_2$, whose partial pressure is $8 \times 10^{-10}$ mbar, i.e. 2 L/h. Thus, the poisoning

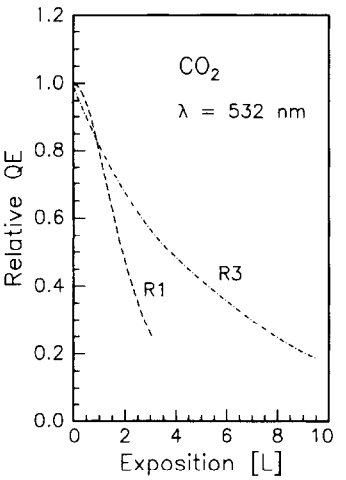


Fig. 4. Quantum efficiency at 532 nm of the R1 and R3 photocathodes as a function of the exposition to $CO_2$ [14]. In the abscissa is reported the QE relative to the unexposed photocathode.

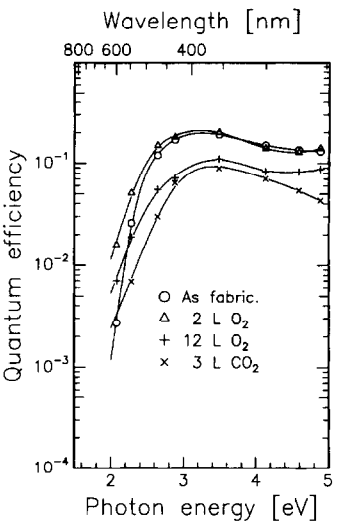


Fig. 6. The spectral responses of the photocathode R1 before and after the exposition to $CO_2$ and $O_2$. The exposition of 2 L of $O_2$ maximizes the QE at 532 nm.

rate due to the $CO_2$ alone accounts for the observed short operational lifetime of the R1 photocathode in the RF cavity. Without the RF power, $H_2O$ could be the main contaminant gas, as the partial pressure of $CO_2$ is negligibly low.

The photocathodes R1 and R3 have also been exposed to $O_2$. In Fig. 5 is shown, as a function of the $O_2$ exposition, the QE of the two photocathodes at two different wavelengths, namely 597 and 532 nm. The photocathode R1 shows a large peak in the QE at 532 nm after 2 L of $O_2$ exposition. The peak is even larger at 597 nm, where the QE increases by a factor of 6, but in this case the maximum QE is reached after 3 L of $O_2$

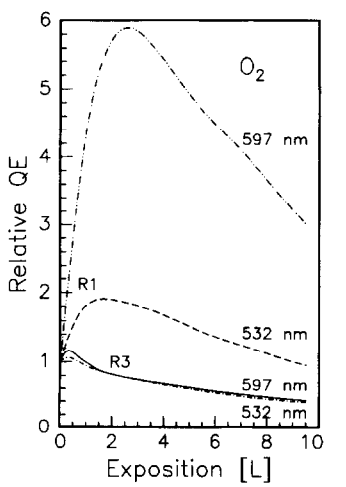


Fig. 5. Quantum efficiency at 597 and 532 nm of the R1 and R3 photocathodes as a function of the exposition to $O_2$ [14]. The QE is reported relative to the unexposed photocathode.

exposition. The presence of such a maximum indicates that the superficial oxidation is the superposition of two effects: the reduction of the surface barrier due to the formation of a Cs–O surface dipole layer and the poisoning effect which changes the electronic structure of the photocathode, effectively reducing the number of photoelectrons produced by the photoemissive material. They both have effect at all wavelength, but the former is more favourable for the slow electrons.

The effect of the oxidation on the photocathode R3 is less remarkable. The maximum gain in QE is below 10% at 597 nm, and the poisoning effect predominates. It is plausible that the last evaporation of K prescribed by R3 prevents the formation of the Cs–O surface dipole layer.

The spectral response of the photocathodes R1 and R3 for different gases and exposures are shown in Fig. 6 and Fig. 7, respectively. After the exposition to 2 L of $O_2$, the spectral response of the photocathode R1 matches quite exactly that of the photocathode R3 "as fabricated".

## 5. Conclusions

We developed few fabrication procedures for thin-film, high QE photoemitters on metallic substrate, suitable for the utilization as pulsed electron sources in high-brightness RF guns, where the vacuum conditions are far from being ideal for these kind of materials.

Two substrates have been tested, namely Mo and stainless steel (AISI 316 LN). Auger depth profiling measurements indicate that the photoemissive film is continuous when stainless steel is used as a substrate, whereas island formation has been observed on Mo

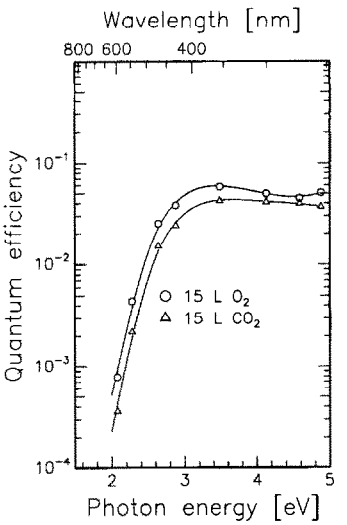


Fig. 7. Spectral responses of the photocathode R3 after the exposition to $CO_2$ and $O_2$.

substrates. The role of the preliminary cleaning procedure in the film formation mechanism remains unclear.

The cause of the short operating lifetime of the bialkali photocathodes has been identified in the poisoning from the $CO_2$ which is desorbed by the RF power from the cavity walls. $CH_4$, $N_2$ and CO exposition up to $10^3$ L, as well as the laser illumination, have no effect on the photocathode lifetime.

The long-wavelength response of the R1 photocathodes may be significantly improved by the exposition to few L of $O_2$. This behaviour has not been observed for the R3 photocathodes.

## Acknowledgements

This work was partially supported by the Human Capital and Mobility contract no. ERB CHRX CT 94055, entitled "High Current Photoemission and Bright Injectors".

## References

[1] A.H. Sommer, Photoemissive Materials (Krieger, New York, 1968).
[2] W.H. Carrol, J. Phys. Chem. Solids 26 (1965) 191.
[3] R.L. Sheffield, E.R. Gray and J.S. Fraser, Nucl. Instr. and Meth. A 272 (1988) 222.
[4] A. Michalke et al., EPAC-92 Conf. Proc., Berlin, Germany, 1992, p. 1014.
[5] C. Travier, Nucl. Instr. and Meth. A 304 (1991) 285.
[6] P. Michelato, P. Gallina and C. Pagani, Nucl. Instr. and Meth. A 340 (1994) 176.
[7] B.M. van Oerle and G.J. Ernst, Nucl. Instr. and Meth. A 358 (1995) 287.
[8] S.H. Kong, J. Kinross-Wright, D.C. Nguyen and R.L. Sheffield, Nucl. Instr. and Meth. A 358 (1995) 272.
[9] R.A. Powell, W.E. Spicer, G.B. Fisher and P. Gregory, Phys. Rev. B 8 (1973) 3987.
[10] E. Chevallay, J. Durand, S. Hutchins, G. Suberlucq and M. Wurgel, Nucl. Instr. and Meth. A 340 (1994) 146.
[11] S.H. Kong, J. Kinross-Wright, D.C. Nguyen and R.L. Sheffield, J. Appl. Phys. 77 (1995) 603; S.H. Kong, D.C. Nguyen, R.L. Sheffield and B.A. Sherwood, Nucl. Instr. and Meth. A 358 (1995) 276.
[12] R. Dei-Cas et al., Nucl. Instr. and Meth. A 296 (1990) 209.
[13] P. Michelato, C. Pagani, D. Sertore and S. Valeri, EPAC-94 Conf. Proc. (World Scientific, Singapore, 1994) Vol. 2, p. 1456.
[14] S. Valeri, M.G. Lancellotti, A. di Bona, U. del Pennino, C. Mariani, M. Sancrotti, C. Pagani and P. Michelato, EPAC-94 Conf. Proc., Vol. 2 (World Scientific, Singapore, 1994) p. 1459.
[15] A. di Bona, F. Sabary, S. Valeri, P. Michelato, D. Sertore and G. Suberlucq, J. Appl. Phys. 80 (1996) 3024.